

AN IMPROVED SERRE MODEL: EFFICIENT SIMULATION AND COMPARATIVE EVALUATION

J. S. A. DO CARMO, J. A. FERREIRA, L. PINTO AND G. ROMANAZZI

ABSTRACT: The so-called Serre or Green & Naghdi equations are a well-known set of fully nonlinear and weakly dispersive equations that describe the propagation of long surface waves in shallow water. In order to extend its range of application to intermediate water, some modifications have been proposed in the literature. In this work, we analyze a new Serre model with improved linear dispersion characteristics. This new Serre system, herein denoted by $\text{Serre}_{\alpha,\beta}$, presents additional terms of dispersive origin, thus extending its applicability to more general depth to wavelength ratios.

A careful development of the $\text{Serre}_{\alpha,\beta}$ model allows a straightforward and efficient numerical implementation. This model is suitable for numerical integration by a splitting strategy which requires the solution of a hyperbolic problem and a dispersive problem. The hyperbolic part is discretized using a high order finite volume method. For the dispersive part standard finite differences are used. A set of numerical experiments are conducted to validate the $\text{Serre}_{\alpha,\beta}$ model and to test the robustness of our numerical scheme. Theoretical solutions and benchmark experimental data are used. Moreover, comparisons against the classical Serre equations and against another well established Serre model with improved dispersion characteristics are also made.

KEYWORDS: Serre equations, Dispersion properties, Intermediate water, Numerical simulation, Splitting method, Finite volume, Finite difference.

1. Introduction

Coastal areas are attractive for human settlement and have great economic and social importance. Therefore, the preservation and monitoring of coastal and estuarine regions is of utmost interest. The mathematical modeling of water wave dynamics is crucial for many nearshore phenomena. For instance, wave propagation plays an important role in erosion and sediment transport [5]. The design of shoreline structures, like breakwaters and jetties, also requires an accurate understanding of wave propagation in complex media. Due to its flexibility and low cost, in comparison with physical models,

Received April 10, 2017.

This work was partially supported by the Centre for Mathematics of the University of Coimbra - UID/MAT/00324/2013, funded by the Portuguese Government through FCT/MEC and co-funded by the European Regional Development Fund through the Partnership Agreement PT2020. L. Pinto was also supported by FCT scholarship SFRH/BPD/112687/2015.

mathematical modeling and simulation is a convenient and valuable tool to support engineering projects. For instance, in [14], mathematical models for wave dynamics were used to help in the design of a new dissipation platform to protect the fortification of *S. Lourenço da Cabeça Seca*. This fortification, located at the mouth of the Tagus estuary (Lisbon, Portugal) was built in the end of the XVI century, and is threatened by the continuous action of waves and currents. Another example is the development of new protective jetties for the port of Figueira da Foz, Portugal [12].

In a general setting, the propagation of water waves is governed by a subset of the Navier-Stokes equations with the assumptions of non-compressibility, irrotationality, and perfect fluid, commonly known as Euler equations. Due to the inherent complexity of this system of equations, whose practical applications require efficient information processing and a large amount of data to be stored, several simplified versions have been proposed. Three of the most common ones are the Saint-Venant, the Boussinesq, and the Serre or Green & Naghdi equations [4, 33, 31]. Basically, two types of effects are present in nearshore wave dynamics: nonlinear effects and dispersive effects. The Saint-Venant system is a nonlinear set of equations which is able to describe the nonlinear transformation of some types of waves. This system is suitable for real-world applications, however, due to the total absence of dispersive properties it is not capable of describing wave shoaling and wave propagation over long periods of analysis. In comparison, the Boussinesq system presents better dispersion properties, but its applicability requires some restriction about the nonlinearity. In particular, the Boussinesq equations assume small wave amplitudes. The Serre equations, a so-called fully nonlinear and weakly dispersive system are a set of equations that include the Saint-Venant and the Boussinesq equations as particular cases [10]. Unlike the Boussinesq equations they are suited for strongly nonlinear wave propagation. However, like the Boussinesq equations, they are only applicable to shallow water weakly dispersive wave processes. Therefore, they are not accurate for some complex problems, such as wave propagation over uneven bathymetry where highly dispersive waves can arise as a consequence of nonlinear interactions. These limitations make the Serre standard system not accurate enough for real world nearshore wave dynamics.

To avoid the drawbacks of the classical Serre equations, several improvements were proposed throughout the years. Also extensions to wave breaking problems have been subject of intensive research (see [2] for a recent survey).

Our main goal in the present work is to extend the applicability of the Serre equations by improving their dispersive properties. We observe that some early studies were conducted in this direction. For instance in [38, 19], following the methodology of [30], the dispersion characteristics were improved by replacing the depth-averaged velocity by a dependent variable. Other common methodology to improve the Serre model consists in the addition of terms of dispersive origin. Used first to improve the Boussinesq equations [27], this approach was later adapted to the Serre model in [11]. Following similar arguments a different Serre model with improved dispersion properties was also derived in [3]. Other related alternative models are given in [6, 24]. Following a different concept, an improved model was recently proposed in [8] for flat bottoms. In what concerns numerical simulation finite difference methods were, until very recently, the most usual approach [11, 38, 19]. Lately, the combination of finite difference and finite volume was used in [3, 6, 24] and finite element and discontinuous Galerkin methods were proposed in [28, 18] and [16], respectively. Emphasis should be given to the fact that these methods are mainly restricted to one dimensional problem. One exception is [24] where the method of [6] was extended to two dimensions, but only for cartesian meshes. We refer also to [17] where a discontinuous Galerkin method on simplicial unstructured meshes was used to solve a new class of asymptotically equivalent Serre equations. It should be also mentioned that due to their simpler form the Boussinesq equations have received far more attention in the literature than the Serre equations.

The rest of the paper is organized as follows. For completeness a short derivation of the classical Serre equations is included in the next section. In Section 3, and following the ideas of [11], we derive our improved Serre equations, that we call Serre $_{\alpha,\beta}$ model. This model has the same precision as the classical Serre, up to same order of accuracy, but has improved dispersion characteristics. Another well-know Serre model with improved dispersion properties, herein designated as Serre $_{\theta}$, is also presented. The new numerical strategy used to solve the proposed model is given in Section 4. The following Section 5 is dedicated to numerical experiments. Here, the numerical scheme is tested and the Serre $_{\alpha,\beta}$ model is validated. Numerical comparisons against the classical and the extended Serre $_{\theta}$ models are also given. Finally, in Section 6, some conclusions are drawn.

2. Classical Serre Model

In this section we briefly derive the classical Serre equations referring to [13, 32, 7] to more details. We consider a three-dimensional fluid flow with horizontal velocity $u(x, y, z, t)$, transverse velocity $v(x, y, z, t)$ and vertical velocity $w(x, y, z, t)$. By $p(x, y, z, t)$ we represent the pressure in the fluid. We assume a constant in time bathymetry $b = b(x, y)$ and denoting by h_0 the reference depth we define the vertical height $h(x, y, t) = h_0 + \eta(x, y, t) - b(x, y)$, with $\eta = \eta(x, y, t)$ the free surface elevation. Moreover, let us denote by a the typical wave amplitude and by L the horizontal length scale. We also introduce the parameter of frequency, $\sigma = h_0/L$, and the parameter of nonlinearity, $\epsilon = a/h_0$. In the following we use the dimensionless variables $x = x/L$, $y = y/L$, and $z = z/h_0$. In our coordinate system the axes x and y coincide with the free surface at rest and the z axis is positive upward.

The classical Serre equations are derived from the momentum equations assuming an incompressible, inviscid, and irrotational fluid, and neglecting surface stress. The incompressibility and irrotationality assumptions are equivalent to

$$u_x + v_y + w_z = 0 \quad (1)$$

and

$$u_z = \sigma^2 w_x, \quad v_z = \sigma^2 w_y, \quad v_x = u_y, \quad (2)$$

respectively. The momentum equations are as follows,

$$\begin{aligned} \epsilon u_t + \epsilon^2 (uu_x + vv_y + ww_z) &= -p_x \\ \epsilon v_t + \epsilon^2 (uv_x + vv_y + ww_z) &= -p_y \\ \epsilon \sigma^2 w_t + \epsilon^2 \sigma^2 (uw_x + vw_y + ww_z) &= -p_z - 1. \end{aligned} \quad (3)$$

The system of equations (1)-(3) is complemented with the boundary conditions

$$\begin{aligned} w &= \sigma^2 u b_x + \sigma^2 v b_y, & \text{at the bottom, } z &= -1 + \sigma^2 b \\ w &= \eta_t + \epsilon u \eta_x + \epsilon v \eta_y, & \text{at the free surface, } z &= \epsilon \eta \\ p &= 0, & \text{at the free surface, } z &= \epsilon \eta. \end{aligned}$$

Integrating (1)-(3) over the water depth, this three-dimensional system becomes two-dimensional in the variables

$$\bar{u}(x, y, t) = \int_0^z u(x, y, z, t) dz \quad \text{and} \quad \bar{v}(x, y, t) = \int_0^z v(x, y, z, t) dz.$$

Next, assuming the shallow water condition $\sigma \ll 1$, and expanding the variables in terms up to $O(\sigma^2)$, it can be shown that the new variables \bar{u} , \bar{v} , and w satisfy

$$\begin{aligned}
 h_t + (h\bar{u})_x + (h\bar{v})_y &= 0 \\
 \bar{u}_t + \bar{u}\bar{u}_x + \bar{v}\bar{u}_y + g\eta_x + [(2/3)h_x + (1/2)b_x]P \\
 &\quad + (1/3)hP_x + h_xQ + (1/2)hQ_x = 0 \\
 \bar{v}_t + \bar{u}\bar{v}_x + \bar{v}\bar{v}_y + g\eta_y + [(2/3)h_y + (1/2)b_y]P \\
 &\quad + (1/3)hP_y + h_yQ + (1/2)hQ_y = 0,
 \end{aligned} \tag{4}$$

where g is the gravitational acceleration and

$$\begin{aligned}
 P &= h(\bar{A}^2 - \bar{u}\bar{A}_x - \bar{v}\bar{A}_y - \bar{A}_t) \\
 Q &= w_t + \bar{u}w_x + \bar{v}w_y,
 \end{aligned}$$

with $w = \bar{u}b_x + \bar{v}b_y$ and $\bar{A} = \bar{u}\eta_x + \bar{v}\eta_y$.

The set of equations (4) is known as Serre [33] or Green and Naghhi [21] equations. The one-dimensional version of these equations is written as

$$\begin{cases} h_t + (hu)_x = 0 \\ u_t + uu_x + g\eta_x + \Omega u_t - hh_x u_{xt} - \frac{h^2}{3}(u_{xxt} - u_x u_{xx} + uu_{xxx}) \\ -hh_x uu_{xx} + [h(u_x)^2 + b_{xx}u^2]\eta_x + (\Omega + hb_{xx})uu_x + \frac{h}{2}b_{xxx}u^2 = 0, \end{cases} \tag{5}$$

with

$$\Omega(v) = (h_x b_x + b_x^2 + \frac{h}{2}b_{xx})v \tag{6}$$

and where we have dropped, for simplicity of presentation, the bar over the variable u . Note that (5) is a fully nonlinear set of equations, since no assumption was made on the nonlinearity parameter ϵ . We observe that the well-known Boussinesq equations [4] are obtained from (1)-(3) assuming that $O(\epsilon) = O(\sigma^2)$, or equivalently, $O(\epsilon) \ll 1$. Therefore, the weakly nonlinear Boussinesq equations are only suitable for waves of small relative amplitude. In one dimension the Boussinesq equations are defined by

$$\begin{cases} h_t + (hu)_x = 0 \\ u_t + uu_x + g\eta_x + (h_0 - b)(b_x u_{xt} + \frac{1}{2}b_{xx}u_t - \frac{1}{3}(h_0 - b)u_{xxt}) = 0. \end{cases}$$

Let us also mention that neglecting all the terms of dispersive origin, i.e., keeping terms only up to $O(1)$ in σ , we obtain the Saint-Venant system [31]

$$\begin{cases} h_t + (hu)_x = 0 \\ u_t + uu_x + g\eta_x = 0. \end{cases} \quad (7)$$

Multiplying the second equation of (7) by h , and using the fact that $h_t = -(hu)_x$ and $\eta_x = h_x + b_x$, we can rewrite (7) in the equivalent form

$$\begin{cases} h_t + (hu)_x = 0 \\ (hu)_t + (hu^2 + \frac{1}{2}gh^2)_x + ghb_x = 0. \end{cases} \quad (8)$$

3. The Improved Serre $_{\alpha,\beta}$ Model

In this section we establish the new Serre $_{\alpha,\beta}$ model. In a first step, we rewrite the Serre system (5) in an equivalent but computationally more convenient form. This new formulation allows us to also obtain the new system in a form suitable for numerical purposes.

Following the steps that led to (8), it can be shown that (5) admits the equivalent representation

$$\begin{cases} h_t + (hu)_x = 0 \\ (hu)_t + (hu^2 + \frac{1}{2}gh^2)_x + ghb_x + hT(u_t) + hQ(u) = 0, \end{cases} \quad (9)$$

where T and Q are defined by

$$T(v) = -\frac{h^2}{3}v_{xx} - hh_xv_x + (b_x\eta_x + \frac{h}{2}b_{xx})v, \quad (10)$$

and

$$\begin{aligned} Q(v) = & -\frac{h^2}{3}vv_{xxx} - hh_xvv_{xx} + (b_x\eta_x + \frac{h}{2}b_{xx})vv_x + h\eta_x(v_x)^2 \\ & + \frac{h^2}{3}v_xv_{xx} + hb_{xx}vv_x + \eta_xb_{xx}v^2 + \frac{h}{2}b_{xxx}v^2. \end{aligned}$$

Note that Q presents derivatives of third order in u , what can lead to numerical instabilities [3]. To overcome this issue we note that

$$T(vv_x) = -\frac{h^2}{3}vv_{xxx} - hh_xvv_{xx} + (b_x\eta_x + \frac{h}{2}b_{xx})vv_x - hh_x(v_x)^2 - h^2v_xv_{xx},$$

which allows the computation of $Q(v)$ using $T(vv_x)$ by

$$Q(v) = T(vv_x) + hh_x(v_x)^2 + h^2v_xv_{xx} + h\eta_x(v_x)^2 + \frac{h^2}{3}v_xv_{xx} + hb_{xx}vv_x + \eta_xb_{xx}v^2 + \frac{h}{2}b_{xxx}v^2,$$

or equivalently

$$Q(v) = T(vv_x) + h(h_x + \eta_x)(v_x)^2 + \frac{4h^2}{3}v_xv_{xx} + hb_{xx}vv_x + (\eta_xb_{xx} + \frac{h}{2}b_{xxx})v^2.$$

Therefore, we can recast (9) as

$$\begin{cases} h_t + (hu)_x = 0 \\ (hu)_t + (hu^2 + \frac{1}{2}gh^2)_x + ghb_x + hT(u_t + uu_x) + hQ(u) = 0, \end{cases} \quad (11)$$

with T given by (10) and Q redefined by

$$Q(v) = h(2h_x + b_x)(v_x)^2 + \frac{4}{3}h^2v_xv_{xx} + hb_{xx}vv_x + (\eta_xb_{xx} + \frac{h}{2}b_{xxx})v^2.$$

Let us assume that $h \neq 0$. Defining $T_{\frac{1}{h}}(v) = T(\frac{v}{h})$ and adding and subtracting $hT(g\eta_x)$ to the second equation of (11), we can write the Serre system in the following form

$$\begin{cases} h_t + (hu)_x = 0 \\ (I + hT_{\frac{1}{h}})((hu)_t + (hu^2 + \frac{1}{2}gh^2)_x + ghb_x) - hT(g\eta_x) + hQ(u) = 0, \end{cases} \quad (12)$$

where I denotes the identity operator.

Remark 3.1 Note that third order derivatives are still present in (12) through $T_{\frac{1}{h}}((hu)_t)$. However, from the numerical point of view, this formulation is more efficient because these derivatives do not need to be explicitly calculated.

3.1. Functional splitting. Note that system (12) can be seen as an update of the hyperbolic nonlinear Saint-Venant system (8) using the dispersive terms $hT_{\frac{1}{h}}((hu)_t + (hu^2 + \frac{1}{2}gh^2)_x + ghb_x) - hT(g\eta_x) + hQ(u)$. This fact motivates the splitting of the Serre system (12) into two coupled problems where the hyperbolic nature of the solution of the Saint-Venant system is corrected by a dispersive system. In order to do that, let us denote by Δt the uniform

time step associated with the time grid $\{t_n, n = 0, \dots, N\}$, with $t_n = n\Delta t$, and let $h_{SV}(t)$, $u_{SV}(t)$ be defined by the Saint-Venant system

$$\begin{cases} (h_{SV})_t + (h_{SV}u_{SV})_x = 0 \\ (h_{SV}u_{SV})_t + (h_{SV}u_{SV}^2 + \frac{1}{2}gh_{SV}^2)_x + gh_{SV}b_x = 0, & t \in (t_n, t_{n+1}], \\ h_{SV}(t_n) = h(t_n), u_{SV}(t_n) = u(t_n), \end{cases} \quad (13)$$

where $h(t_n)$, $u(t_n)$ are assumed to be known. Let also $h_d(t)$, $u_d(t)$ be defined by the initial value problem

$$\begin{cases} (h_d)_t = 0 \\ (I + h_d T_{\frac{1}{h_d}})((h_d u_d)_t - h_d T(g\eta_{d,x}) + h_d Q(u_d) = 0, & t \in (t_n, t_{n+1}], \\ h_d(t_n) = h_{SV}(t_{n+1}), u_d(t_n) = u_{SV}(t_{n+1}). \end{cases} \quad (14)$$

Then, the splitting approximation to the solution $h(t_{n+1})$, $u(t_{n+1})$ of the Serre system (12) is taken to be $h(t_{n+1}) \simeq h_d(t_{n+1})$, $u(t_{n+1}) \simeq u_d(t_{n+1})$.

To represent in a more convenient way the defined splitting solution we introduce the following notations:

$$\begin{aligned} (h_d(t_{n+1}), u_d(t_{n+1})) &= S_d(h_{SV}(t_n), u_{SV}(t_n)), \\ (h_{SV}(t_{n+1}), u_{SV}(t_{n+1})) &= S_{SV}(h(t_n), u(t_n)). \end{aligned}$$

Using these notations we are able to represent the solution of the previous functional splitting in the following equivalent form

$$(h(t_{n+1}), u(t_{n+1})) \simeq S_d(S_{SV}(h(t_n), u(t_n))) := S_d \circ S_{SV}(h(t_n), u(t_n)).$$

System (14) can be replaced by a new one with improved dispersive properties. We follow the approach used in [11], in which terms of dispersive origin were added and subtracted to the classical Serre equations. In particular, we add and subtract to the second equation of (14) the term $h_d T_{\frac{1}{h_d}}^{\alpha, \beta}((h_d u_d)_t)$, with

$$T^{\alpha, \beta}(v) = -\beta \frac{h^2}{3} v_{xx} - \alpha h h_x v_x + \alpha (b_x \eta_x + \frac{h}{2} b_{xx}) v.$$

Moreover, using the classical approximation, $u_{d,t} = -g\eta_{d,x}$, we find the problem

$$\begin{cases} (h_d)_t = 0 \\ (I + h_d T_{\frac{1}{h_d}} + h_d T_{\frac{1}{h_d}}^{\alpha, \beta})((h_d u_d)_t) - h_d (T - T^{\alpha, \beta})(g\eta_{d,x}) + h_d Q(u_d) = 0 \\ h_d(t_n) = h_{SV}(t_{n+1}), u_d(t_n) = u_{SV}(t_{n+1}), \end{cases} \quad (15)$$

for $t \in (t_n, t_{n+1}]$. The solution of (15) is now denoted by $S_d^{\alpha,\beta}(h_{SV}, u_{SV})$. Using the coupling $S_d^{\alpha,\beta} \circ S_{SV}$ we define the proposed $\text{Serre}_{\alpha,\beta}$ model. Moreover, another coupling can be obtained if we replace (15) by a new problem that can be established following the approach described in [3]. It is given by

$$\begin{cases} (h_d)_t = 0 \\ (I + h_d \theta T_{\frac{1}{h_d}})((h_d u_d)_t) - h_d T(g \eta_{d,x}) + h_d Q(u_d) = 0, & t \in (t_n, t_{n+1}], \\ h_d(t_n) = h_{SV}(t_{n+1}), u_d(t_n) = u_{SV}(t_{n+1}), \end{cases}$$

with θ constant. If the solution of the previous problem is denoted by $S_d^\theta(h_{SV}, u_{SV})$, then $S_d^\theta \circ S_{SV}$ defines the well-known Serre_θ model.

Remark 3.2 We emphasize that the solutions $S_d^{\alpha,\beta}(h_{SV}, u_{SV})$, $S_d^\theta(h_{SV}, u_{SV})$ and $S_d(h_{SV}, u_{SV})$ are equivalent up to order $O(\sigma^2)$. We note that $S_d(h_{SV}, u_{SV})$ can be obtained from $S_d^{\alpha,\beta}(h_{SV}, u_{SV})$ considering $\alpha = \beta = 0$ and from $S_d^\theta(h_{SV}, u_{SV})$ taking $\theta = 1$.

In this work we employ a Strang second order splitting [34]. Before presenting this new splitting we introduce some notation. By $S_{SV}(\Delta t)(h, u)$, $S_{SV}(\Delta t)(h_d, u_d)$, $S_d(\Delta t)(h_{SV}, u_{SV})$, $S_d^{\alpha,\beta}(\Delta t)(h_{SV}, u_{SV})$, and $S_d^\theta(\Delta t)(h_{SV}, u_{SV})$ we denote the solutions $S_{SV}(h, u)$, $S_{SV}(h_d, u_d)$, $S_d(h_{SV}, u_{SV})$, $S_d^{\alpha,\beta}(h_{SV}, u_{SV})$, and $S_d^\theta(h_{SV}, u_{SV})$, respectively. The Strang splitting solution at t_{n+1} defined, for instance, by $S_d^{\alpha,\beta}(h_{SV}, u_{SV})$, is then obtained from

$$S_{SV}\left(\frac{\Delta t}{2}\right) \circ S_d^{\alpha,\beta}(\Delta t) \circ S_{SV}\left(\frac{\Delta t}{2}\right)(h, u)(t_n), \quad (16)$$

that is, from the composition of iii with ii and i, where

$$\text{i. } \begin{cases} (h_{SV})_t + (h_{SV} u_{SV})_x = 0 \\ (h_{SV} u_{SV})_t + (h_{SV} u_{SV}^2 + \frac{1}{2} g h_{SV}^2)_x + g h_{SV} b_x = 0, & t \in (t_n, t_{n+1/2}], \\ h_{SV}(t_n) = h(t_n), u_{SV}(t_n) = u(t_n), \end{cases}$$

with $t_{n+1/2} = t_n + \frac{\Delta t}{2}$,

$$\text{ii. } \begin{cases} (h_d)_t = 0 \\ (I + h_d T_{\frac{1}{h_d}} + h_d T_{\frac{1}{h_d}}^{\alpha,\beta})((h_d u_d)_t) - h_d (T - T^{\alpha,\beta})(g \eta_{d,x}) + h_d Q(u_f) = 0 \\ h_d(t_n) = h_{SV}(t_{n+1/2}), u_d(t_n) = u_{SV}(t_{n+1/2}), \end{cases}$$

for $t \in (t_n, t_{n+1}]$, and

$$\text{iii. } \begin{cases} (h_{SV})_t + (h_{SV}u_{SV})_x = 0 \\ (h_{SV}u_{SV})_t + (h_{SV}u_{SV}^2 + \frac{1}{2}gh_{SV}^2)_x + gh_{SV}b_x = 0, & t \in (t_{n+1/2}, t_{n+1}], \\ h_{SV}(t_{n+1/2}) = h_d(t_{n+1}), u_{SV}(t_{n+1/2}) = u_d(t_{n+1}), \end{cases}$$

The approximation to the solution $h(t_{n+1}), u(t_{n+1})$ is then $h(t_{n+1}) \simeq h_{SV}(t_{n+1}), u(t_{n+1}) \simeq u_{SV}(t_{n+1})$. We call this last splitting the $\text{Serre}_{\alpha, \beta}$ model. The Strang splitting obtained by replacing $S_d^{\alpha, \beta}$ by S_d^θ is called the Serre_θ model, while the one obtained by replacing $S_d^{\alpha, \beta}$ by S_d is called the Serre model.

Remark 3.3 Some effort has been made to estimate the optimal value of the parameters α, β , and θ associated with the extended Serre systems. Usually, this analysis is carried out using linearized systems. Note that a number of simplifications and assumptions are involved in this type of analysis and they are not problem independent. For further discussion on this subject we refer to [11, 3, 25, 26].

4. A Coupled Finite Volume - Finite Difference Method

The functional splitting allows us to use in the numerical simulation methods well adapted to each subproblem. In our case, for the hyperbolic Saint-Venant problem, we use a finite volume method in space while for the dispersive problems that define $S_d^{\alpha, \beta}, S_d^\theta$, or S_d solutions we use a classical finite difference method in space. The time integration will be performed using a Runge-Kutta method. Details of the proposed numerical scheme are given next.

4.1. Discretization of the Saint-Venant system. For clarity, let us write again the Saint-Venant system (8), it is given by,

$$\begin{cases} (h_{SV})_t + (h_{SV}u_{SV})_x = 0 \\ (h_{SV}u_{SV})_t + (h_{SV}u_{SV}^2 + \frac{1}{2}gh_{SV}^2)_x + gh_{SV}b_x = 0, & t \in (t_n, t_{n+1}]. \end{cases} \quad (17)$$

Next, we briefly describe the high order finite volume method used to solve system (17) and we refer to [22, 23] for further details.

Let us define $w = h + b$ and $q = hu$. Where, for simplicity, we have dropped the subscript SV . Using this notation and the fact that $b_t = 0$ we can rewrite

(17) in the equivalent form

$$\begin{cases} w_t + q_x = 0 \\ q_t + \left(\frac{q^2}{w-b} + \frac{g}{2}(w-b)^2 \right)_x = -g(w-b)b_x. \end{cases} \quad (18)$$

Moreover, defining

$$U = [w, q]^T, \quad F(U, b) = \left(q, \frac{q^2}{w-b} + \frac{g}{2}(w-b)^2 \right)^T,$$

and

$$S(U, b) = (0, -q(w-b)_x)^T,$$

we obtain the usual conservative form

$$U_t + F(U, b)_x = S(U, b). \quad (19)$$

Without loss of generality we assume that the spatial domain is $[0, 1]$ and let $\{x_j = j\Delta x, j = 1, \dots, N, x_1 = \Delta x, x_N = 1 - \Delta x\}$ be a uniform grid in this spatial domain, where Δx represents the uniform mesh step size. Following the traditional finite volume approach, we integrate (19) over a finite volume cell $I_j = [x_{j-1/2}, x_{j+1/2}]$, obtaining

$$(\bar{U}_j)_t = -\frac{H_{j+1/2} - H_{j-1/2}}{\Delta x} + \bar{S}_j, \quad j = 1, \dots, N; t \in (t_n, t_{n+1}]. \quad (20)$$

In (20), \bar{U}_j represents the approximation defined by the midpoint rule of the respective integral, i.e.,

$$\bar{U}_j \approx \frac{1}{\Delta x} \int_{I_j} U(x, t) dx,$$

and \bar{S}_j the approximation

$$\bar{S}_j \approx \frac{1}{\Delta x} \int_{I_j} S(U(x, t), b(x, t)) dx$$

to be defined later. To give the expression of $H_{j\pm 1/2}$ we introduce the piecewise linear reconstruction \tilde{U}_j defined by

$$\tilde{U}_j(x) = \bar{U}_j + (U_x)_j(x - x_j), \quad x_{j-1/2} < x < x_{j+1/2},$$

where $(U_x)_j$ denotes the numerical slope obtained by the generalized minmod limiter

$$(U_x)_j = \text{minmod} \left(\delta \frac{\bar{U}_j - \bar{U}_{j-1}}{\Delta x}, \frac{\bar{U}_{j+1} - \bar{U}_{j-1}}{2\Delta x}, \delta \frac{\bar{U}_{j+1} - \bar{U}_j}{\Delta x} \right),$$

with $\delta \in [1, 2]$ and

$$\text{minmod}(z_1, z_2, \dots) = \begin{cases} \min_j \{z_j\}, & \text{if } z_j > 0, \forall j, \\ \max_j \{z_j\}, & \text{if } z_j < 0, \forall j, \\ 0, & \text{otherwise.} \end{cases}$$

Then the central-upwind numerical fluxes are given by

$$H_{j+1/2} = \frac{a_{j+1/2}^+ F(U_{j+1/2}^-, b_{j+1/2}) - a_{j+1/2}^- F(U_{j+1/2}^+, b_{j+1/2})}{a_{j+1/2}^+ - a_{j+1/2}^-} + \frac{a_{j+1/2}^+ a_{j+1/2}^-}{a_{j+1/2}^+ - a_{j+1/2}^-} (U_{j+1/2}^+ - U_{j+1/2}^-),$$

where $U_{j+1/2}^\pm$ are given by $\tilde{U}_j(x_{j+1/2} + 0)$ and $\tilde{U}_{j+1}(x_{j+1/2} - 0)$, i.e., the right and the left values at $x = x_{j+1/2}$, respectively, and the local propagation speeds $a_{j+1/2}^\pm$ are determined by

$$a_{j+1/2}^+ = \max\{u_{j+1/2}^+ + \sqrt{gh_{j+1/2}^+}, u_{j+1/2}^- + \sqrt{gh_{j+1/2}^-}, 0\},$$

$$a_{j+1/2}^- = \max\{u_{j+1/2}^+ - \sqrt{gh_{j+1/2}^+}, u_{j+1/2}^- - \sqrt{gh_{j+1/2}^-}, 0\}.$$

Finally the source term in (20), \bar{S}_j , is given by

$$\bar{S}_j^{(2)} = -g \frac{(b(x_{j+1/2}) - b(x_{j-1/2}))(w_{j+1/2}^- - b(x_{j+1/2})) + w_{j-1/2}^+ - b(x_{j-1/2}))}{2\Delta x}.$$

This discretization of the source term ensures that the method is well balanced, meaning that it is stable for steady state solutions of system (18) as well as their small perturbations [22]. A few remarks are now in order.

Remark 4.1 The role of the minmod limiter is to ensure the stability of the numerical solution avoiding the creation of spurious oscillations near step fronts. The parameter δ controls the amount of numerical dissipation, with larger values corresponding to a less dissipative numerical scheme, but more prone to oscillations. The optimal value of δ is problem dependent, in this work we used $\delta = 1.3$. For a review on the minomd limiter and other limiters we refer to [29, 35, 36].

Remark 4.2 This scheme can be easily modified to handle discontinuous bottoms and also to be positivity preserving [22, 23]. This last property

is particular important for problems where the water height is almost zero ($h \sim 0$). Since in this work we do not consider applications with almost dry states or discontinuous bottoms, we found the proposed method adequate and reliable enough.

Remark 4.3 This finite volume method is theoretically second order accurate for sufficiently smooth solutions, but it may reduce, as usual, to a first order method near step fronts or discontinuities. Note that when the min-mod limiter is equal to zero the proposed scheme reduces to the first order upwind scheme.

System (20) is now rewritten as

$$\bar{U}'(t) = F_{FV,\Delta t}(\bar{U}(t)), \quad t \in (t_n, t_{n+1}]. \quad (21)$$

For the time discretization of the ordinary differential system (21) a third order strong stability preserving (SSP) Runge-Kutta method is applied. By employing a third order method we ensure that the second order of the splitting approach (16) is preserved.

Explicit SSP methods like the one used here have proven to be well adapted to solve hyperbolic problems. In particular they present better stability properties, with no extra computational cost, when compared with other explicit methods of equivalent order [20]. For the differential problem (21) our SSP method can be written as follows

$$\begin{aligned} \bar{U}^{(1)} &= \bar{U}^n + \Delta t F_{FV,\Delta t}(\bar{U}^n), \\ \bar{U}^{(2)} &= \frac{3}{4}\bar{U}^n + \frac{1}{4}\bar{U}^{(1)} + \frac{1}{4}\Delta t F_{FV,\Delta t}(\bar{U}^{(1)}), \\ \bar{U}^{n+1} &= \frac{1}{3}\bar{U}^n + \frac{2}{3}\bar{U}^{(2)} + \frac{2}{3}\Delta t F_{FV,\Delta t}(\bar{U}^{(2)}), \end{aligned} \quad (22)$$

where Δt is the time step and where \bar{U}^n and \bar{U}^{n+1} are the approximations for $\bar{U}(t_n)$ and $\bar{U}(t_{n+1})$, respectively.

To simplify the presentation of the discrete version of the Strang splitting (16) we denote the previous solution computed at time level t_{n+1} by

$$\bar{U}^{n+1} = S_{FV}(\Delta t)(\bar{U}^n),$$

this leads to

$$(h_{SV}^{n+1}, u_{SV}^{n+1}) = S_{FV}(\Delta t)(h_{SV}^n, u_{SV}^n). \quad (23)$$

The Courant-Friedrichs-Lewy stability condition associated with this explicit integration method is given by

$$\Delta t^n = \text{CFL} \frac{\Delta x}{\max_j (\max(a_{j+1/2}^{n,+}, -a_{j+1/2}^{n,-}))}, \quad (24)$$

with CFL less or equal to one [20]. Throughout this work we have used the value $\text{CFL} = 0.5$. Note that to shorten notation we have been assuming that the time step Δt is uniform. However, in fact, the time step is non-uniform; it is defined by (24) and the time grid is given $t_{n+1} = t_n + \Delta t^n$.

4.2. Discretization of the dispersion system. Let us rewrite system (15) in the equivalent form

$$\begin{cases} (h_d)_t = 0 \\ (I + T + T^{\alpha,\beta})(u_d)_t = g(T - T^{\alpha,\beta})\eta_{d,x} - Q(u_d), \quad t \in (t_n, t_{n+1}]. \end{cases} \quad (25)$$

Using the fact that $(h_d)_t = 0$, and dropping for convenience the subscript d , system (25) reduces to the following partial differential equation,

$$(I + T + T^{\alpha,\beta})u_t = g(T - T^{\alpha,\beta})\eta_x - Q(u), \quad (26)$$

with T , $T^{\alpha,\beta}$, and Q given by

$$T(v) = -\frac{h^2}{3}v_{xx} - hh_x v_x + (b_x \eta_x + \frac{h}{2}b_{xx})v,$$

$$T^{\alpha,\beta}(v) = -\beta \frac{h^2}{3}v_{xx} - \alpha hh_x v_x + \alpha (b_x \eta_x + \frac{h}{2}b_{xx})v,$$

and

$$Q(v) = h(2h_x + b_x)v_x^2 + \frac{4}{3}h^2 v_x v_{xx} + hb_{xx} v v_x + (\eta_x b_{xx} + \frac{h}{2}b_{xxx})v^2.$$

The dispersive equation (26) is discretized by standard finite difference technique. To define the scheme we introduce the grid $\{\bar{x}_i = i\Delta x, i = 0, \dots, N, \bar{x}_0 = 0, \bar{x}_N = 1\}$. The finite difference method is obtained by replacing in (26) the second and third spatial derivatives by the following second order approximations

$$\begin{aligned} v_x(\bar{x}_i) &\approx D_c v_i = \frac{v_{i+1} - v_{i-1}}{2\Delta x}, & v_{xx}(\bar{x}_i) &\approx D_2 v_i = \frac{v_{i+1} - 2v_i + v_{i-1}}{\Delta x^2}, \\ v_{xxx}(\bar{x}_i) &\approx D_3 v_i = \frac{-v_{i-2} + 2v_{i-1} - 2v_{i+1} + 2v_{i+2}}{2\Delta x^3}, \end{aligned}$$

where $v_i = v(\bar{x}_i)$, $v_{i\pm 1} = v(\bar{x}_{i\pm 1})$, and $v_{i\pm 2} = v(\bar{x}_{i\pm 2})$.

We remark that when D_2 and D_3 are used near the boundary, fictitious grid points are needed outside of the domain. We define $x_{-2} = -2\Delta x$, $x_{-1} = -\Delta x$, at the left boundary, and $x_{N+2} = 1+2\Delta x$, $x_{N+1} = 1+\Delta x$, at the right boundary. Assuming periodic boundary conditions, we set $v_{-k} = v_{N-k}$ and $v_{N+k} = v_k$, $k = 1, 2$. It is important to observe that the finite difference nodes \bar{x}_i are set at the boundary of the finite volume cell $I_j = [x_{j-1/2}, x_{j+1/2}]$ and therefore do not coincide with the finite volume nodes x_j . Whenever necessary we use cubic interpolation to switch between the finite volume and the finite difference approximation. The use of third order interpolation ensures that no loss of accuracy occurs in this auxiliary step. In what follows we use tilde over variables to denote interpolated values.

Using the finite difference operators D_c , D_2 , and D_3 in T , $T^{\alpha,\beta}$, and Q we get

$$\begin{aligned} T_{\Delta x}(v_i) &= -\frac{(h_i)^2}{3}D_2v_i - h_iD_ch_iD_cv_i + (D_cb_iD_c\eta_i + \frac{h_i}{2}D_2b_i)v_i, \\ T_{\Delta x}^{\alpha,\beta}(v_i) &= -\beta\frac{(h_i)^2}{3}D_2v_i - \alpha h_iD_ch_iD_cv_i + \alpha(D_cb_iD_c\eta_i + \frac{h_i}{2}D_2b_i)v_i, \end{aligned}$$

and

$$\begin{aligned} Q_{\Delta x}(v_i) &= h_i(2D_ch_i + D_cb_i)(D_cv_i)^2 + \frac{4}{3}(h_i)^2D_cv_iD_2v_i \\ &\quad + h_iD_2b_iv_iD_cv_i + (D_c\eta_iD_2b_i + \frac{h_i}{2}D_3b_i)(v_i)^2. \end{aligned}$$

Considering the previous approximations in (26) we obtain

$$(I + T_{\Delta x} + T_{\Delta x}^{\alpha,\beta})\bar{u}'_{d,i}(t) = g(T_{\Delta x} - T_{\Delta x}^{\alpha,\beta})D_c\eta_i(t) - Q_{\Delta t}(\bar{u}_{d,i}(t)),$$

for $t \in (t_n, t_{n+1}]$, $i = 1, \dots, N$, and with $\bar{u}_{d,i}(t)$ the numerical approximation at \bar{x}_i for $u_d(t)$. This can be written as

$$\begin{cases} \bar{u}'_d(t) = F_{FD}(\bar{u}_d(t)), & t \in (t_n, t_{n+1}] \\ \bar{u}_d^n = \tilde{u}_{SV}^{n+1/2}. \end{cases} \quad (27)$$

For the time discretization of (27) we adopt again the SSP Runge-Kutta method (22). After the time integration in $[t_n, t_{n+1}]$ we get u_d^{n+1} .

The finite difference discretization of the dispersion equation (25) and the time integration of (27) leads to h_d^{n+1} , u_d^{n+1} being this solution represented

by

$$(h_d^{n+1}, u_d^{n+1}) = S_{FD}^{\alpha, \beta}(\Delta t)(h_d^n, u_d^n). \quad (28)$$

We recall that $h_d^n = \tilde{h}_{SV}^{n+1/2}$, $u_d^n = \tilde{u}_{SV}^{n+1/2}$, where $\tilde{h}_{SV}^{n+1/2}$ and $\tilde{u}_{SV}^{n+1/2}$ are determined by cubic interpolation of $h_{SV}^{n+1/2}$ and $u_{SV}^{n+1/2}$, respectively. Note also that from the first equation of (25) we get $h_d^{n+1} = h_d^n$.

The corresponding approximation for the Serre $_{\theta}$ model can be obtained adapting the procedures that led to (28). This solution is represented by

$$(h_d^{n+1}, u_d^{n+1}) = S_{FD}^{\theta}(\Delta t)(h_d^n, u_d^n). \quad (29)$$

4.3. Fully discrete Strang splitting method. The numerical approximation for the Serre $_{\alpha, \beta}$ solution defined by (16) at time level t_{n+1} is then obtained coupling the finite volume solution (23) with the finite difference approximation (28) by the following Strang splitting method

$$\begin{aligned} \text{i. } \left\{ \begin{array}{l} (h_{SV}^{n+1/2}, u_{SV}^{n+1/2}) = S_{FV}(h_{SV}^n, u_{SV}^n) \\ h_{SV}^n = h^n, u_{SV}^n = u^n, \end{array} \right. & \quad \text{ii. } \left\{ \begin{array}{l} (h_d^{n+1}, u_d^{n+1}) = S_{FD}^{\alpha, \beta}(h_d^n, u_d^n) \\ h_d^n = \tilde{h}_{SV}^{n+1/2}, u_d^n = \tilde{u}_{SV}^{n+1/2}, \end{array} \right. \\ \text{iii. } \left\{ \begin{array}{l} (h_{SV}^{n+1}, u_{SV}^{n+1}) = S_{FV}(h_{sv}^{n+1/2}, u_{SV}^{n+1/2}) \\ h_{SV}^{n+1/2} = \tilde{h}_d^{n+1}, u_{SV}^{n+1/2} = \tilde{u}_d^{n+1}. \end{array} \right. \end{aligned}$$

The Strang splitting method that leads to an approximation for Serre $_{\theta}$ is defined analogously replacing the second step ii by

$$\left\{ \begin{array}{l} (h_d^{n+1}, u_d^{n+1}) = S_{FD}^{\theta}(h_d^n, u_d^n) \\ h_d^n = \tilde{h}_{SV}^{n+1/2}, u_d^n = \tilde{u}_{SV}^{n+1/2}. \end{array} \right.$$

5. Numerical Experiments

In this section we present some numerical results that intent to show the performance of our numerical approach as well as to validate the proposed Serre $_{\alpha, \beta}$ model. For that we consider three examples, namely:

1. A solitary wave traveling over a flat plane with a known analytic solution;
2. A solitary wave traveling up a slope and reflection on a vertical wall with available experimental data;
3. A periodic wave traveling over an irregular underwater bar with available experimental data.

The first theoretical example aims to test the stability and convergence properties of our numerical scheme. In the next two examples we use experimental data available in the literature. Our intention is not only to illustrate the behavior of our splitting scheme using real laboratory data but also to make a comparison between the classical Serre model, the extended Serre $_{\theta}$ model, and the proposed extended Serre $_{\alpha,\beta}$ model.

5.1. Example 1: Solitary wave over a flat plane. We are not aware of any theoretical solution for the extended Serre $_{\alpha,\beta}$ system. However, for the classical Serre system (12), which is obtained setting $\alpha = \beta = 0$ in system (15), some analytical solutions have been derived. Considering flat bathymetry $b = 0$, one of such solutions is expressed in a form of the solitary wave

$$h(x, t) = h_0 + a(\operatorname{sech}(K(x - Ct - x_0)))^2, \quad u = C\left(1 - \frac{h_0}{h}\right),$$

where h_0 is the water depth at rest, x_0 is the initial position of the wave crest, a is the wave amplitude, and C and K are constants defined by $C = c_0\sqrt{1 + a/h_0}$ and $K = \sqrt{3a/(4h_0^2(h_0 + a))}$, with $c_0 = \sqrt{gh_0}$.

For our experiment we set the spatial domain $[0, 250]$ (m) and the parameters $x_0 = 25$ (m), $h_0 = 1$ (m), and $a/h_0 = 0.6$. The spatial mesh step size used in the simulation was $\Delta x = 0.05$ (m). In what concerns boundary conditions, periodic ones were used. In Figure 1 and Figure 2 we present the numerical solution at time $t = 50$ (s) of the free surface elevation η and of the velocity u , respectively. The theoretical solution at the same time as well as the initial condition are also displayed. It is observed that the wave amplitude and speed are correctly reproduced by the proposed numerical method and no numerical instability is visible. More rigorously, at $t = 50$ (s) the root-mean square error (RMSE) for η and u is equal to 0.00017 (m) and to 0.00044 (m/s), respectively. The RMSE is given by

$$\text{RMSE} = \left(\frac{1}{N} \sum_{i=1}^N (v_i^n - v(x_i, t_n))^2 \right)^{1/2},$$

where v_i^n represents the numerical approximation at the mesh point x_i and time t_n of the exact solution $v(x_i, t_n)$.

To further highlight the robustness and accuracy of our splitting method we also compare our results with the results presented in [11] where a cumbersome finite difference method was used to solve the Serre system in the

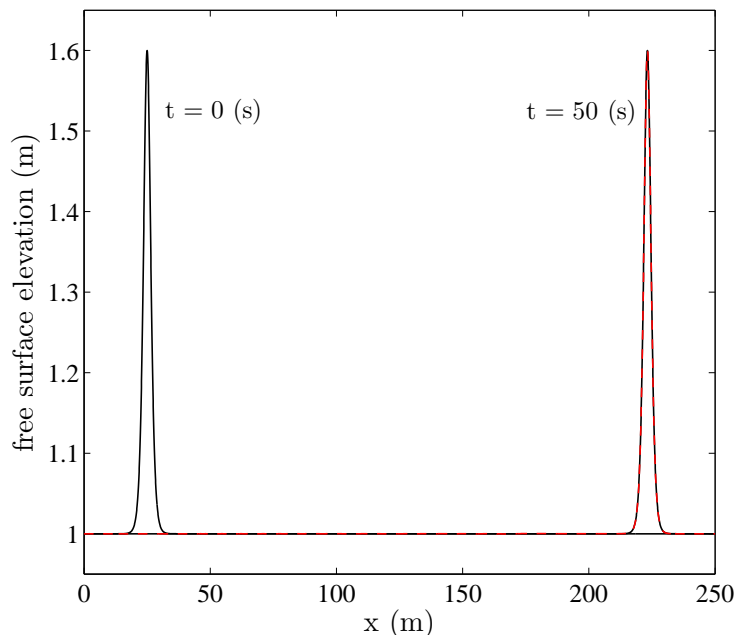


FIGURE 1. Numerical solution of free surface elevation η at time $t = 50$ (s) (red dash line) and analytical solution at time $t = 0$ (s) and time $t = 50$ (s) (black solid line).

compact form (5). For instance, in what concerns the RMSE of η , the value reported in [11] was 0.0007 (m), this is more than four times higher than our value, 0.00017 (m). Note that the value $\Delta x = 0.05$ (m) was used in both cases. In the next experiment we estimate the convergence rate of the numerical method with respect to the L_∞ -norm. For that we fix $T = 5$ (s) and vary the size of the spatial mesh step size Δx . We denote by

$$E_k^\eta = \max_{i=1,\dots,N} |\eta_i^n - \eta(x_i, t_n)|, \quad k = 1, \dots, 4,$$

the error of the free surface elevation at the mesh $\Delta x_k = 0.4, 0.2, 0.1, 0.05$. To calculate the numerical order of convergence we use the expression

$$\text{rate} = \log_2 \frac{E_k^\eta}{E_{k+1}^\eta}.$$

The results given in Table 1 confirm the expected second order convergence rate. Here, we use the notation E_k^u to denote the error for the velocity u .

5.2. Example 2: Solitary wave traveling up a slope with reflection on a vertical wall. For our second example we consider the already classical

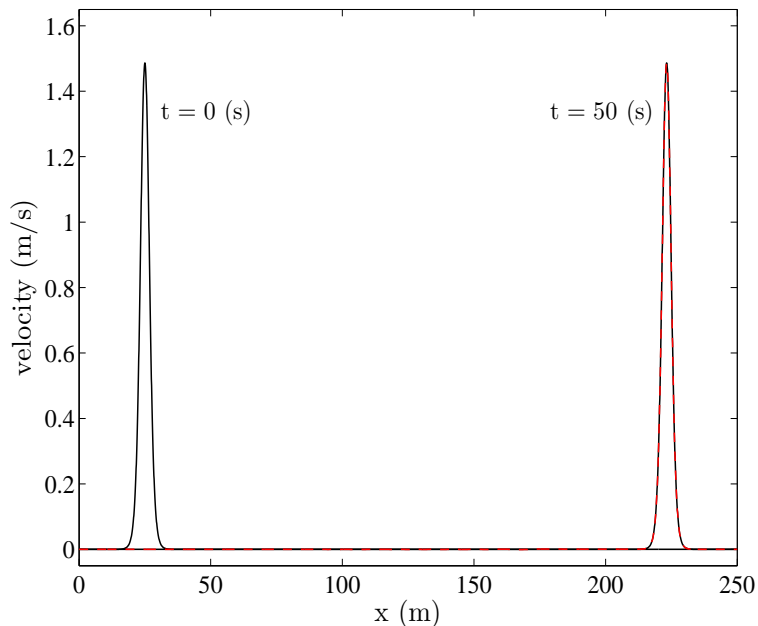


FIGURE 2. Numerical solution of velocity u at time $t = 50$ (s) (red dash line) and analytical solution at time $t = 0$ (s) and time $t = 50$ (s) (black solid line).

Δx_k	E_k^η	rate	E_k^u	rate
0.4	0.165	-	0.315	-
0.2	0.0434	1.927	0.0860	1.873
0.1	0.0110	1.980	0.0235	1.872
0.05	0.00265	2.053	0.00587	2.000

TABLE 1. Numerical estimation of the convergence rate.

experiment reported in [15, 37]. The goal of such experiment was to study the behavior of a wave traveling up a slope with reflection on a vertical wall. We take the bathymetry profile shown in Figure 3 and consider a solitary wave initially centered at $x = 25$ (m) and with an amplitude of $a = 0.12$ (m). The wave propagates from left to right with velocity u obtained from the equation given in previous Example 1. As depicted in Figure 3 the wave climbs a slope before being reflected by an impermeable wall. The slope starts at $x = 55$ (m) and ends at $x = 75$ (m) precisely where the wall is located. The water depth at rest is 0.70 (m). In this simulation we consider fully reflecting boundary conditions [3] at the right boundary, which

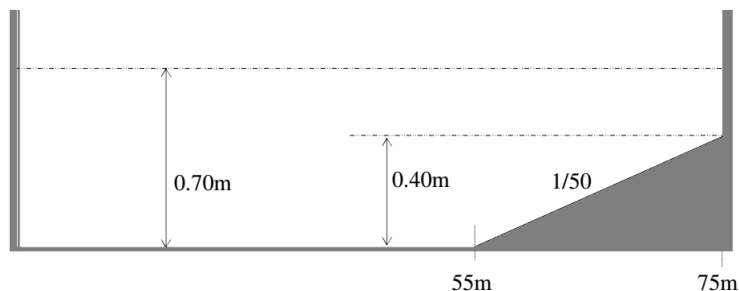


FIGURE 3. Bottom topography associated with Example 2.

corresponds to the impermeable wall. To avoid wave reflections from the left boundary we extend the computational domain. The spatial step size is set to $\Delta x = 0.05$ (m). This value was empirically chosen based on the accuracy of the results. The experimental data available corresponds to the evolution over time of the free surface elevation η at the point $x = 72.75$ (m).

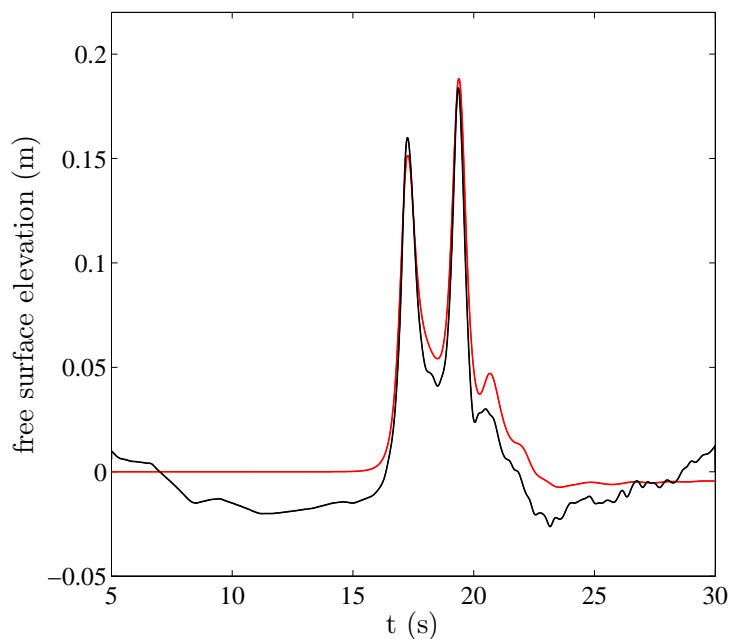


FIGURE 4. Time evolution of free surface elevation η at $x = 72.75$ (m); numerical solution with the Serre model (red line) and experimental data (black line).

In the following we compare the experimental data with numerical results obtained with our improved $\text{Serre}_{\alpha,\beta}$ model. First we consider $\alpha = \beta = 0$, which corresponds to the classical Serre system. The results for the free

surface elevation are given in Figure 4. As can be seen a good agreement between numerical and experimental data is observed. The phase discrepancy is of about 0.017 (s) for the first peak and of about 0.026 (s) for the second peak. The RMSE for the wave height at the first and the second peak is equal to 0.0086 (m) and 0.0044 (m), respectively. Visually, these results are similar to those obtained in [3, 28].

As already mentioned, the $\text{Serre}_{\alpha,\beta}$ model is only relevant in intermediate water conditions, and when dispersive effects play a key role. Therefore, for this experiment, it is not expected that it leads to a big improvement. Nevertheless, we used exhaustive search optimization to find the parameters α and β that minimize the phase and height errors at the two peaks. For $\alpha = 0.01$ and $\beta = 0.017$ the phase error was 0 (s) and the height error at the first and the second peak was equal to 0.0073 (m) and 0.0064 (m), respectively. This is illustrated in Figure 5. On the other hand, we were not able to significantly decrease the height error without increasing the phase error already obtained with the Serre model.

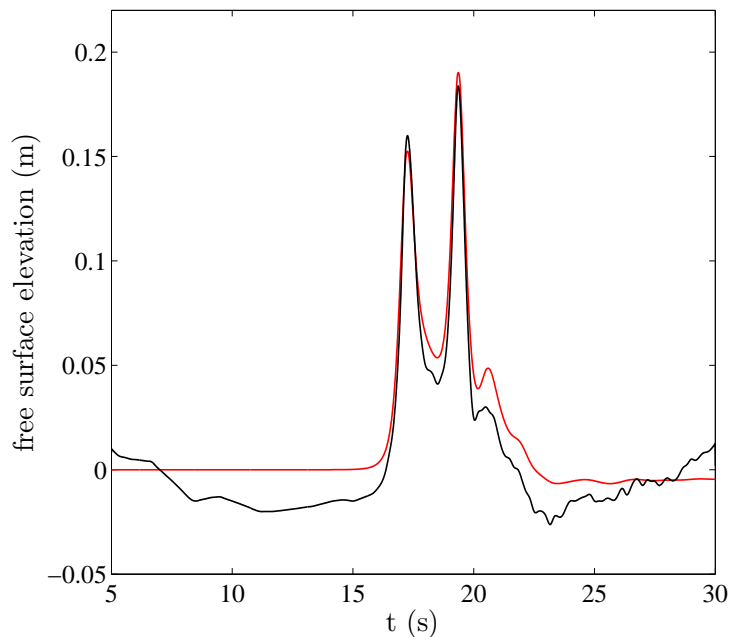


FIGURE 5. Time evolution of free surface elevation η at $x = 72.75(\text{m})$; numerical solution with the $\text{Serre}_{\alpha,\beta}$ model ($\alpha = 0.01$ and $\beta = 0.017$) (red line) and experimental data (black line).

We also conducted tests with the extended Serre_{θ} model. We were able to reduce the phase error to 0 (s) considering $\theta = 1.11$. In this case the

total height error at the peaks was 0.017 (m). We remark that for the same phase error we were able to obtain an inferior height error with our model, namely 0.015 (m) (see Table 2). Note also that for any θ value the height error given by this model was always superior to the one already given by the Serre model. These findings are summarized in Table 2. The results for Serre_θ are not shown since they are identical to those for $\text{Serre}_{\alpha,\beta}$.

	Parameters			Height Error (m)			Phase Error (s)		
	α	β	θ	1st Peak	2nd Peak	Total	1st Peak	2nd Peak	Total
Serre	0	0	-	0.0086	0.0044	0.013	0.017	0.026	0.043
Serre_θ	-	-	1.11	0.0068	0.0096	0.017	0	0	0
$\text{Serre}_{\alpha,\beta}$	0.01	0.017	-	0.0075	0.0064	0.015	0	0	0

TABLE 2. Comparison for Example 2 between the Serre and the extended Serre models.

5.3. Example 3: Periodic wave over an underwater bar. In our last example we consider the experiment reported in [1] (see also [9]) and whose experimental setup is shown in Figure 6. As can be seen this setup consists of a wave flume with 25 (m) long with an underwater bar of 11 (m) located between the 6th and 17th (m) of the flume. In the first 6 (m), the trapezoidal bar presents a positive slope of 1:20 followed by a 2 (m) horizontal crest and a downstream slope of 1:10. The water height before and after the bar is

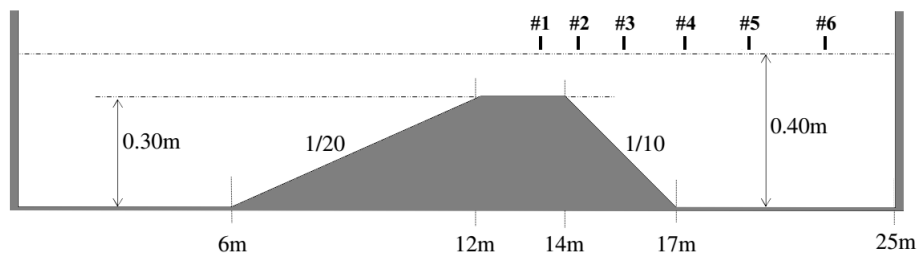


FIGURE 6. Bottom topography of Example 3 and location of the gauges.

equal to 0.40 (m) reducing to 0.1 (m) at the top of the bar. At the left boundary periodic waves are generated using an hydraulically driven piston-type wavemaker. Experimental free surface measurements were acquired using a series of wave gauges placed through the channel. The location of the gauges is identified in Figure 6, with numbers from 1 to 6, and the precise

location of the gauges is 13.5, 14.5, 15.7, 17.3, 19, and 21 (m), respectively. For our purpose the last three gauges, after the wave interaction with the underwater bar, are particularly relevant.

According to [1] the experimental wave height was 0.02 (m), while the period and the wavelength were 2.02 (s) and 3.73 (m), respectively. To simulate this type of wave we set an input condition at the left boundary. For the free surface elevation η we use the expression

$$\eta(0, t) = \cos(2\pi ft)a$$

where a is the wave amplitude and f is the wave frequency. For the velocity u the following equation was used

$$u(0, t) = \frac{g}{2\pi f} \tanh\left(\frac{2\pi h_0}{\lambda}\right) \frac{1}{h_0} \eta(0, t)$$

with λ the wavelength. At the right boundary, to avoid non physical reflections, the computational domain was extended. To discretize the domain a mesh step size of $\Delta x = 0.02$ (m) was used. Like in the previous example, Δx was empirically chosen based on the fit of the experimental data. The results of our simulation are depicted in Figure 7 for classical Serre, Figure 8 for Serre_θ , and Figure 9 for $\text{Serre}_{\alpha,\beta}$. In each figure four plots are shown, corresponding to the comparison between the experimental and the numerical data at the gauges 1, 4, 5, and 6. The results are given for the time interval [25, 30] (s) where the wave dynamics are already stabilized. For the Serre_θ and $\text{Serre}_{\alpha,\beta}$ models an exhaustive search optimization was done in order to find the optimal parameters.

The analysis of Figure 7 reveals that the classical Serre system is able to accurately describe the experimental measurements up until gauge 1, located at 13.5 (m). However, at the wave gauges 4, 5, and 6 the discrepancy between numerical predictions and experimental data is significant. This discrepancy becomes more pronounced as the distance between the gauge and the underwater bar increases. As shown in Figure 7 (top image on the left) the regular incident wave shoals and steepens when going up and over the bar, accumulating higher harmonics as the nonlinearity increases. These higher harmonics are released on the downward slope and can be seen as highly dispersive waves. Under these conditions the limitations of the weakly dispersive Serre equations become evident. In fact, a comparison with the Serre_θ (Figure 8) and $\text{Serre}_{\alpha,\beta}$ (Figure 9) models, both having additional terms of dispersive origin, reveals their superiority. This is clear visible at the three

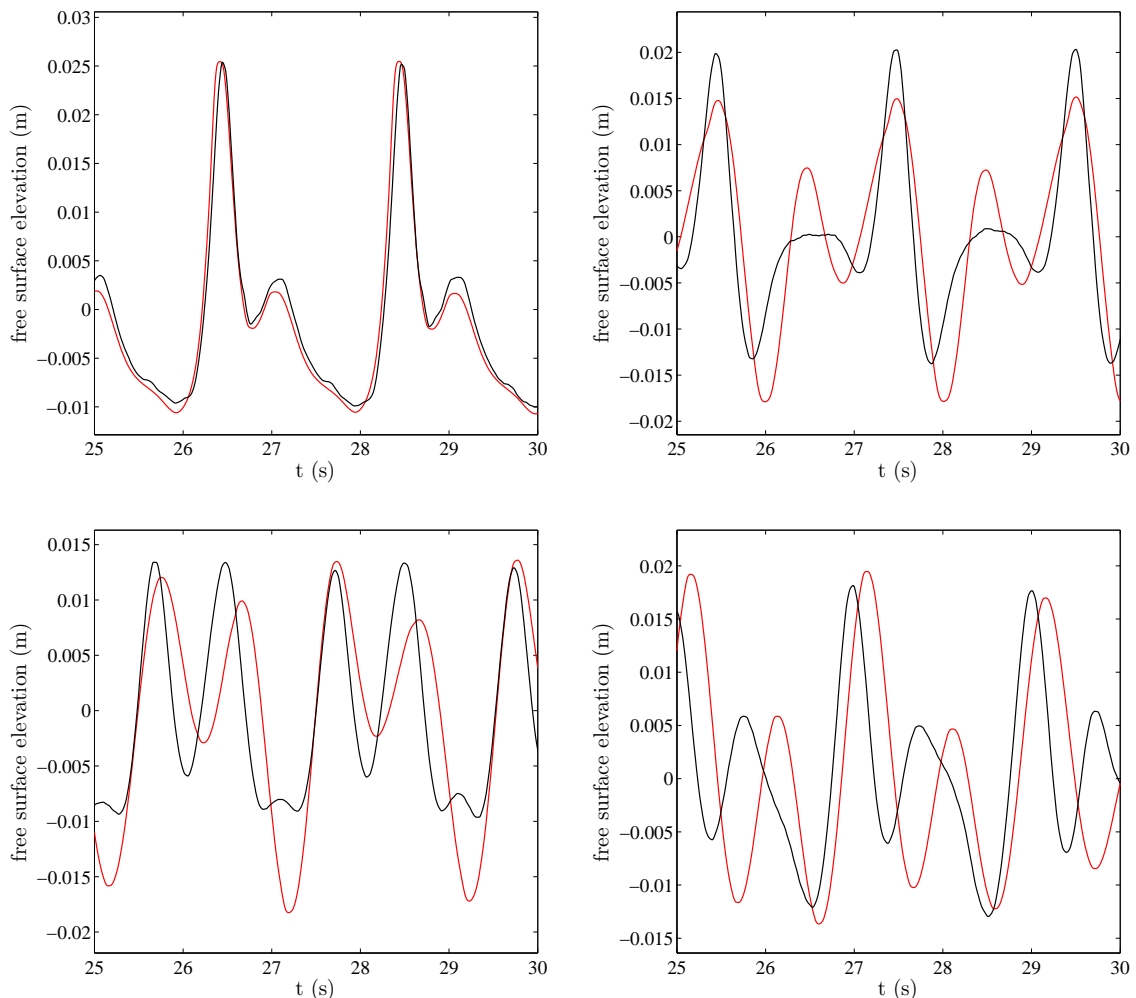


FIGURE 7. From left to right and top to bottom: Time evolution of free surface elevation η at wave gauges 1, 4, 5, and 6; numerical solution obtained with the classical Serre model (red line) and experimental data (black line).

gauges located after the bar. Note that at gauge 1 all three models have a similar and good performance. In what concerns the differences between Serre_θ and $\text{Serre}_{\alpha,\beta}$, it is observed that both models have identical results until gauge 4 located at 17.3 (m). However, at the last two gauges, when the higher harmonics are already fully released, the proposed $\text{Serre}_{\alpha,\beta}$ provides a better agreement with the experimental data. We remark that the results obtained with the Serre_θ model are visually identical to those reported in [24, 6].

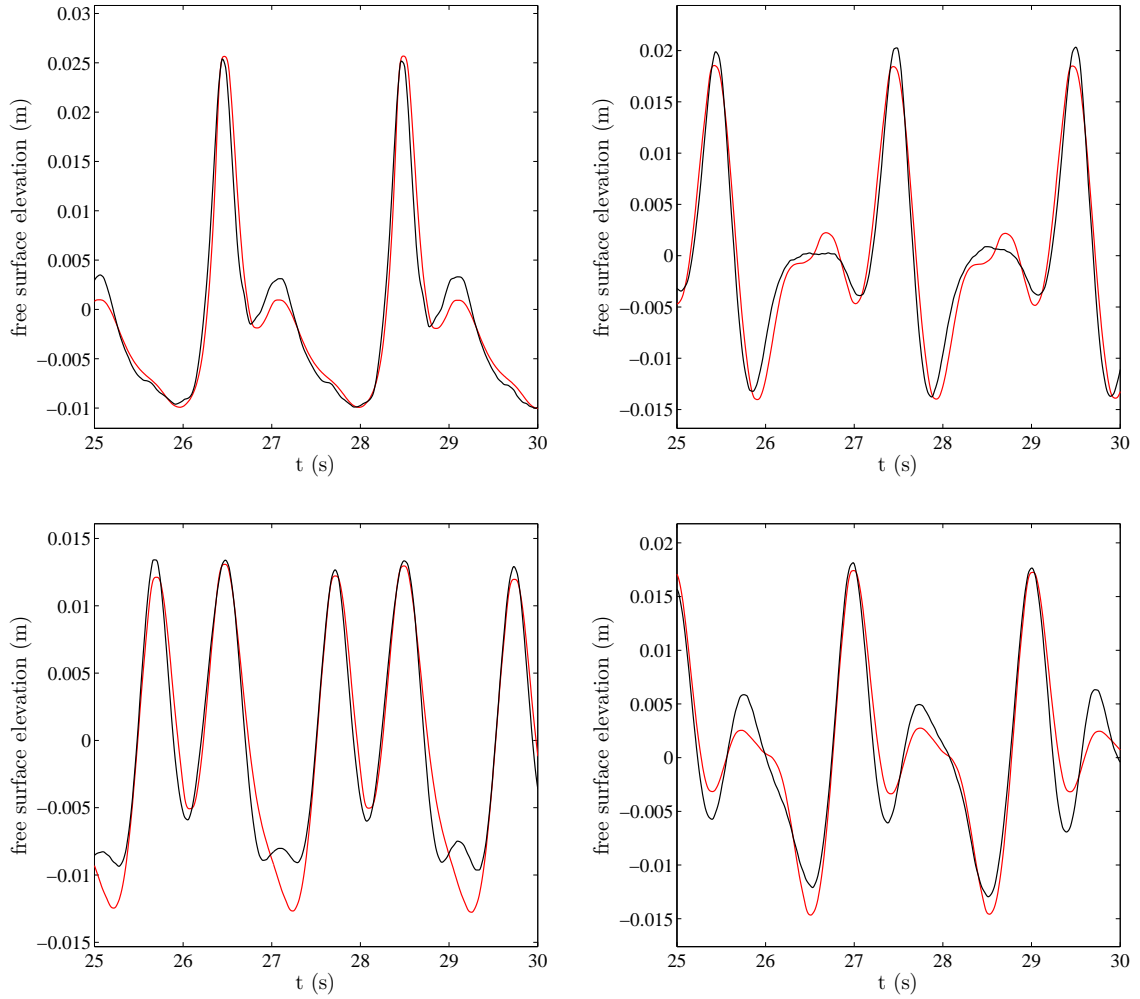


FIGURE 8. From left to right and top to bottom: Time evolution of free surface elevation η at wave gauges 1, 4, 5, and 6; numerical solution obtained with the Serre_θ model with $\theta = 1.14$ (red line) and experimental data (black line).

To better illustrate our discussion we present in Figure 10 the RMSE, for each model, at all gauges (1 to 6). The results displayed in Figure 10 confirm and highlight the superiority of the improved Serre models for highly dispersive waves. The better performance of the proposed $\text{Serre}_{\alpha,\beta}$ is also clear, particularly at the last two gauges where the dispersive waves are more significant.

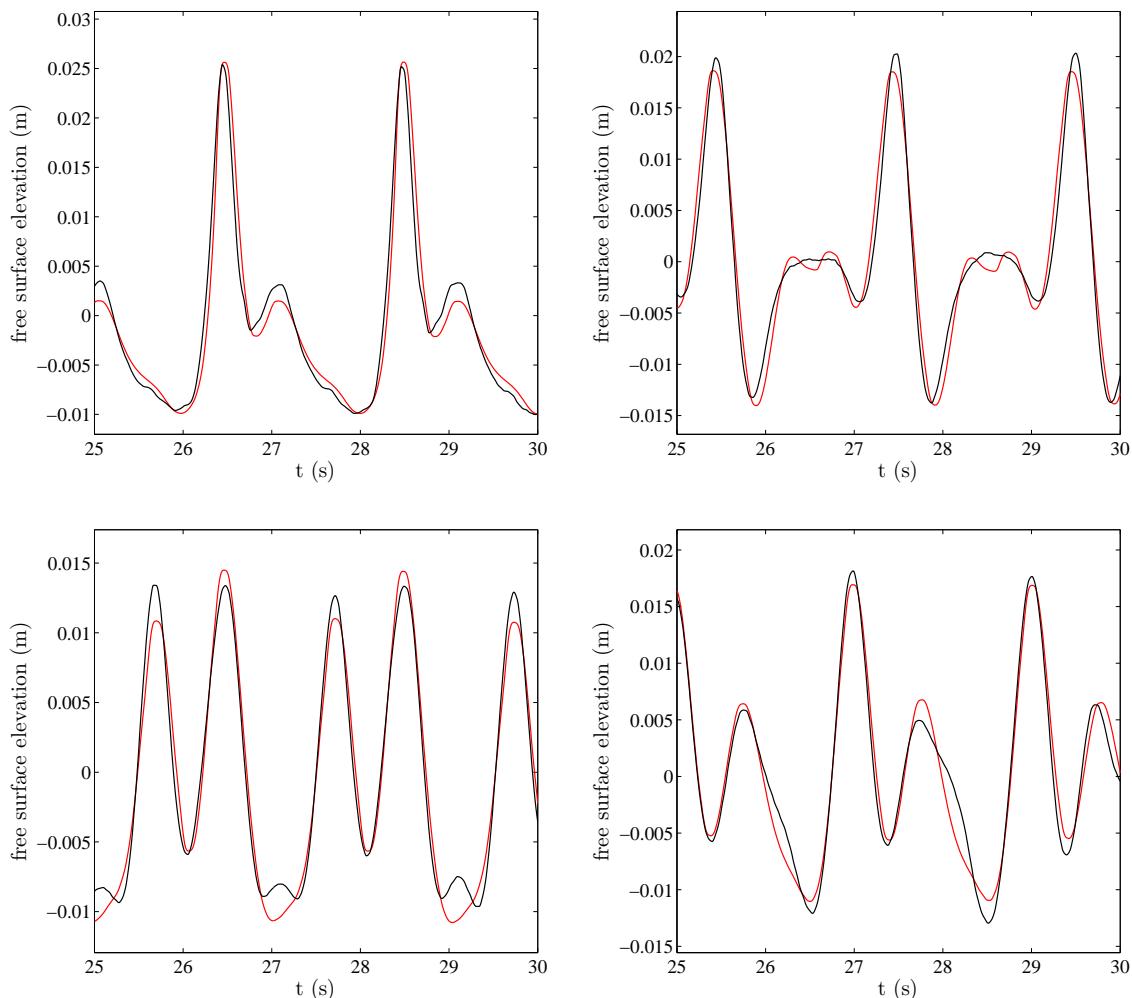


FIGURE 9. From left to right and top to bottom: Time evolution of free surface elevation η at wave gauges 1, 4, 5 and 6; numerical solution obtained with the $\text{Serre}_{\alpha,\beta}$ model with $(\alpha, \beta) = (0.06, 0.055)$ (red line) and experimental data (black line).

6. Conclusion

In this work an efficient numerical strategy for an extended Serre system with improved dispersion properties, denoted by $\text{Serre}_{\alpha,\beta}$, was proposed and tested. Our strategy relies on a splitting scheme where a high order finite volume method is used to discretize the hyperbolic part while a finite difference method is used for the dispersive part. This efficient approach is only possible due to a formulation of the $\text{Serre}_{\alpha,\beta}$ system in a form suitable for these numerical methods. A series of numerical experiments prove the robustness

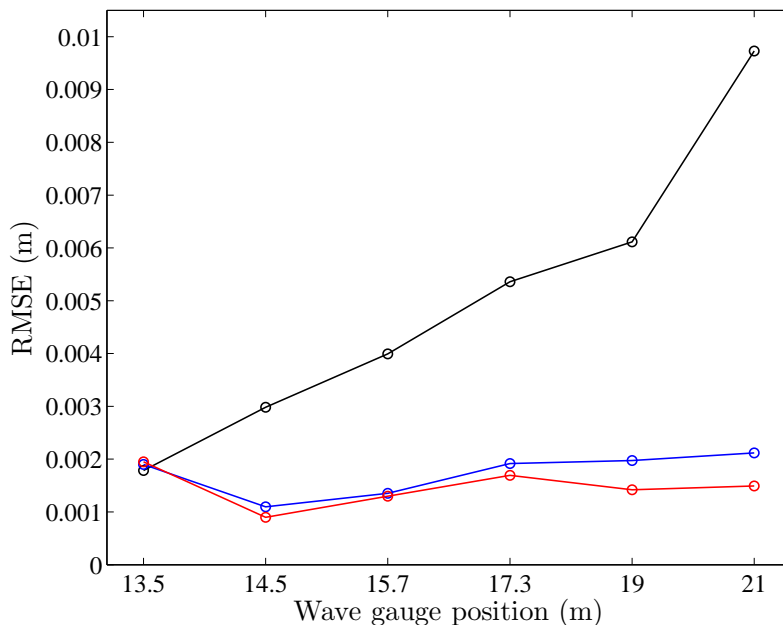


FIGURE 10. Comparison of the RMSE at the six gauge of Example 3; classical Serre (black line), Serre $_{\theta}$ (blue line), and proposed Serre $_{\alpha,\beta}$ (red line).

and accuracy of our strategy. Moreover, using the challenging propagation of regular waves over a submerged bar data [1], we also prove the ability of our model to reproduce strongly dispersive waves propagation. Comparisons with the classical Serre model, as well as with the well established Serre $_{\theta}$ model, illustrate the superiority of the proposed Serre $_{\alpha,\beta}$ model.

Some directions of future research include the extension of our model to two dimensions and the simulation of more demanding problems including dry areas, wave breaking, and run-up processes.

References

- [1] S. Beji and J. A. Battjes. Experimental investigation of wave propagation over a bar. *Coastal Engineering*, 19:151–162, 1993.
- [2] P. Bonneton, E. Barthelémy, F. Chazel, R. Cienfuegos, D. Lannes, F. Marche, and M. Tissier. Recent advances in Serre-Green Naghdi modelling for wave transformation, breaking and runup processes. *European Journal of Mechanics - B/Fluids*, 30:589–597, 2011.
- [3] P. Bonneton, F. Chazel, D. Lannes, F. Marche, and M. Tissier. A splitting approach for the fully nonlinear and weakly dispersive Green-Naghdi model. *Journal of Computational Physics*, 230:1479–1498, 2011.
- [4] J. Boussinesq. Théorie des ondes et des remous qui se propagent le long d’un canal rectangulaire horizontal. *Journal de Mathématiques Pures et Appliquées*, 2:55–108, 1872.

- [5] J. Carreiras, J. .A. do Carmo, and F. Seabra-Santos. Settlement of vertical piles exposed to waves. *Coastal Engineering*, 47:355–365, 2003.
- [6] F. Chazel, D. Lannes, and F. Marche. Numerical simulation of strongly nonlinear and dispersive waves using a Green-Naghdi model. *Journal of Scientific Computing*, 48:105–116, 2011.
- [7] R. Cienfuegos, E. Barthélemy, and P. Bonneton. A fourth-order compact finite volume scheme for fully nonlinear and weakly dispersive Boussinesq-type equations. Part i: Model development and analysis. *International Journal for Numerical Methods in Fluids*, 51:1217–1253, 2006.
- [8] D. Clamond, D. Dutykh, and D. Mitsotakis. Conservative modified Serre-Green-Naghdi equations with improved dispersion characteristics. *Communications in Nonlinear Science and Numerical Simulation*, 42:245–257, 2017.
- [9] M. W. Dingemans. Comparison of computations with Boussinesq-like models and laboratory measurements. *Technical Report H-1684.12*, 1994.
- [10] J. S. do Carmo. Nonlinear and dispersive wave effects in coastal processes. *Journal of Integrated Coastal Zone Management*, 16:343–355, 2016.
- [11] J. S. A. do Carmo. Boussinesq and serre type models with improved linear dispersion characteristics: Applications. *Journal of Hydraulic Research*, 51:719–727, 2013.
- [12] J. S. A. do Carmo and F. J. Seabra-Santos. Numerical solution of the generalized serre equations with the McCormack finite-difference scheme. *International Journal for Numerical Methods in Fluids*, 16:725–738, 1993.
- [13] J. S. A. do Carmo and F. J. Seabra-Santos. On breaking waves and wave-current interaction in shallow water: A 2D H finite element model. *International Journal for Numerical Methods in Fluids*, 22:429–444, 1996.
- [14] J. S. A. do Carmo and F. J. Seabra-Santos. Near-shore sediment dynamics computation under the combined effects of waves and currents. *Advances in Engineering Software*, 33:37–48, 2002.
- [15] N. Dodd. A numerical model of wave run-up, overtopping and regeneration. *Journal of Waterway, Port, Coastal, and Ocean Engineering*, 124:73–80, 1998.
- [16] A. Duran and F. Marche. Discontinuous-Galerkin discretization of a new class of Green-Naghdi equations. *Communications in Computational Physics*, 17:721–760, 2015.
- [17] A. Duran and F. Marche. A discontinuous galerkin method for a new class of Green-Naghdi equations on simplicial unstructured meshes. *Applied Mathematical Modelling*, Available online 16 January 2017, ISSN 0307-904X, <http://doi.org/10.1016/j.apm.2017.01.030>.
- [18] A. G. Filippini, M. Kazolea, and M. Ricchiuto. A flexible genuinely nonlinear approach for nonlinear wave propagation, breaking and run-up. *Journal of Computational Physics*, 310:381–417, 2016.
- [19] M. F. G. Gobbi, J. T. Kirby, and G. Wei. A fully nonlinear Boussinesq model for surface waves. part 2. extension to $o(kh)^4$. *Journal of Fluid Mechanics*, 405:181–210, 2000.
- [20] S. Gottlieb, C.-W. Shu, and E. Tadmor. Strong stability-preserving high-order time discretization methods. *SIAM Review*, 87:89–112, 2001.
- [21] A. E. Green and P. M. Naghdi. A derivation of equations for wave propagation in water of variable depth. *Journal of Fluid Mechanics*, 78:237–246, 1976.
- [22] A. Kurganov and D. Levy. Central-upwind schemes for the Saint-Venant system. *Mathematical Modelling and Numerical Analysis*, 36:397–425, 2002.
- [23] A. Kurganov and G. Petrova. A second-order well-balanced positivity preserving central-upwind scheme for the Saint-Venant system. *Communications in Mathematical Sciences*, 5:133–160, 2007.
- [24] D. Lannes and F. Marche. A new class of fully nonlinear and weakly dispersive Green-Naghdi models for efficient 2D simulations. *Journal of Computational Physics*, 282:238–268, 2015.

- [25] Z. B. Liu and Z. C. Sun. Two sets of higher-order Boussinesq-type equations for water waves. *Ocean Engineering*, 32:1296–1310, 2005.
- [26] P. A. Madsen, H. B. Bingham, and H. Liu. A new Boussinesq method for fully nonlinear waves from shallow to deep water. *Journal of Fluid Mechanics*, 462:1–30, 2002.
- [27] P. A. Madsen, R. Murray, and O. R. Sørensen. A new form of the Boussinesq equations with improved linear dispersion characteristics. *Coastal Engineering*, 15:371–378, 1991.
- [28] D. Mitsotakis, C. Synolakis, and M. McGuinness. A modified Galerkin/finite element method for the numerical solution of the Serre-Green-Naghdi system. *International Journal for Numerical Methods in Fluids*, DOI: 10.1002/fld.4293, 2016.
- [29] H. Nessyahu and E. Tadmor. Non-oscillatory central differencing for hyperbolic conservation laws. *Journal of Computational Physics*, 87:408–463, 1990.
- [30] O. Nwogu. Alternative form of Boussinesq equations for nearshore wave propagation. *Journal of Waterway Port Coastal and Ocean Engineering*, 119:618–638, 1993.
- [31] B. S.-Venant. Theory of unsteady water flow, with application to river floods and to propagation of tides in river channels. *Comptes Rendus*, 73:148–154, 237–240, 1973.
- [32] F. J. Seabra-Santos. As aproximações de Wu e de Green & Naghdi no quadro geral da teoria da água pouco profunda. In *Simpósio Luso-Brasileiro de Hidráulica e Recursos Hídricos (4º SILUSBA)*, 1989.
- [33] F. Serre. Contribution à l’étude des écoulements permanents et variables dans les canaux. *La Houille Blanche*, 8:374–388, 1953.
- [34] G. Strang. On the construction and comparison of difference schemes. *SIAM Journal on Numerical Analysis*, 5:506–517, 1968.
- [35] P. K. Sweby. High resolution schemes using flux limiters for hyperbolic conservation laws. *SIAM Journal on Numerical Analysis*, 21:995–1011, 1984.
- [36] B. van Leer. Towards the ultimate conservative difference scheme. V. a second-order sequel to Godunov’s method. *Journal of Computational Physics*, 32:101–136, 1979.
- [37] M. Walkley and M. Berzins. A finite element method for the one-dimensional extended Boussinesq equations. *International Journal for Numerical Methods in Fluids*, 29:143–157, 1999.
- [38] G. Wei and J. T. Kirby. Time-dependent numerical code for extended Boussinesq equations. *Journal of Waterway Port Coastal and Ocean Engineering*, 121:251–261, 1995.

J. S. A. DO CARMO

IMAR, INSTITUTE OF MARINE RESEARCH, DEP. OF CIVIL ENGINEERING, UNIVERSITY OF COIMBRA, PORTUGAL

E-mail address: jsacarmo@dec.uc.ut

J. A. FERREIRA

CMUC, DEP. OF MATHEMATICS, UNIVERSITY OF COIMBRA, PORTUGAL

E-mail address: ferreira@mat.uc.pt

L. PINTO

CMUC, DEP. OF MATHEMATICS, UNIVERSITY OF COIMBRA, PORTUGAL

E-mail address: luisp@mat.uc.pt

G. ROMANAZZI

DEP. OF APPLIED MATHEMATICS, INSTITUTE OF MATHEMATICS, STATISTICS AND SCIENTIFIC COMPUTING, UNIVERSITY OF CAMPINAS, BRAZIL

E-mail address: roman@ime.unicamp.br